ISSN 1590-8844
International Journal of Mechanics and Control, Vol. XX, No. XX, 20XX

Comparison between hydraulic and bi-stable systems for the mitigation of the end-effector collisions

Matteo Bottin[1*] Giulio Cipriani[*] Alberto Doria [*] Riccardo Minto [*] Giulio Rosati [*]
Domenico Tommasino [*]

[*] Department of Industrial Engineering, University of Padova

ABSTRACT

This paper deals with the development of special end-effectors able to mitigate the effects of collisions on the robot and on the impacted objects. This aim is achieved by avoiding the direct mechanical coupling between the end-effector and the robot flange by means of hydraulic and mechanical systems. The mathematical model of an end-effector equipped with hydraulic chambers connected by an orifice is developed and integrated with the model of a robot with compliance in the approach direction. To make a comparison, the mathematical model of the bi-stable mechanical system is integrated with the same compliant robot. Numerical simulations of one dimensional collisions are carried out. Numerical results show that, if there is a rather long dead time between the impact and the reaction of the robot, the hydraulic system generates smaller forces than the mechanical system and causes smaller initial velocities of the impacted object. Conversely, if the dead time is short, the bi-stable system generates smaller initial velocities of the impacted object and, when the object is fixed, it generates smaller forces on the robot than the hydraulic system.

1 INTRODUCTION

The recent industrial development has led robots to perform much more complex tasks than in the past. With the increase in task complexity, and therefore the development of autonomous and collaborative applications in industrial robotics, it is now necessary to adopt an additional level of safety standards [1, 2].
A first level of safety is provided by collision avoidance strategies [3], which are designed to avoid collisions with the operator in the case of collaborative robots or, more in general, with obstacles and manipulated objects, by properly changing the robot trajectory. In both scenarios, the controller aims to compensate for the environment unpredictability. Therefore, it is necessary for the robot system to detect, or even predict, collision and act accordingly. Several algorithms have been proposed in the literature [4, 5] to overcome this issue. Moreover, learning from demonstration approaches [6] aims to teach the correct path to the robot by means of trial and error approaches.
However, in both scenarios collisions with obstacles and manipulated objects are still possible. Since collisions can happen, the velocity of the robot must be limited, lowering the efficiency of the robotic system. Hence, it is necessary to develop approaches that mitigate the effects of collisions, which can be done introducing compliance into the actuation system [7].
Dills et al. [8] focused on the actuator design to mitigate the effects, with the aim to reduce the impedance output of high-power manipulators used for human-robot interaction. A hybrid configuration which includes DC electric actuators and electromagnetic brakes was adopted. Using a 1 DOF testbed, they evaluated the safety against impacts, indicating that, even with the brake, the system shows accelerations comparable to the ones of series elastic actuators [9]. Ayoubi et al. [10] designed a novel safety mechanism for rotary joints to decouple the inertia of the colliding part of the robot with the inertia of the rest of the robot. The

Contact author: Matteo Bottin[1]
[1], Via Venezia 1 - 35131 Padova, Italy
E-mail: matteo.bottin@unipd.it

approach is based on variable stiffness actuators [11, 12]; in particular, the system is composed of a stiffness generator block, which generates the desired stiffness profile, and a stiffness adjusting block, that adjusts the stiffness profile. A collision with a human operator was simulated, showing that the mechanism maintains a constant contact force during a collision for a wide range of motor torque and inertia, demonstrating the decoupling properties of the mechanism. Sandoval et al. [13] designed a prismatic compliant joint and provided a safety performance evaluation with a simulation of the complaint joint attached to a KUKA iiwa robot. The comparison with rigid joints showed that the magnitude of the impact force, which is used as a safety index, significantly decreases when using the compliant joint. Moreover, simulation tests showed that the impact energy has been absorbed by the compliant joint. Seriani et al. [14] focused on the robot design by proposing a framework for preloaded compliant links. The authors developed a 10-DOF prototype to validate the analytical model, showing a reduction in the oscillations due to high energy impacts. Heng et al. [15] investigated the robot skin solution, by introducing a fluid-driven robot skin which allowed for both sensing functions to detect collisions and damping functions to mitigate the collision. This was achieved by using piezoresistive sensing cells and a pneumatic actuating cell to inflate the skin and mitigate the peak force of the collision. An experimental test showed that filling the skin with high-pressure gas could decrease the peak impact force by about 26%.

Focusing on collaborative robots, they are becoming safer for human-robot collaboration, by featuring torque sensors, torque observers, or tactile skins. However, the focus of these safety approaches lies on the robot; thus, it is necessary to focus on the end-effector to mitigate the impact with the tool [16]. For these reasons, Pantano et al. [17] presented the safety evaluation of a reconfigurable gripper designed for human-robot collaboration. Moreover, they carried out a risk assessment followed by practical safety tests. With respect to collisions, they adopted safety measures in the form of power and force limitations, in particular limiting the operational speed up to 100 mm/s. Jujjavarapu et al. [18] presented a design for a robotic tool based on a variable stiffness mechanism realized with permanent magnets. A hammering task was used to analyze the capabilities of the proposed design to absorb sudden impacts that could damage the robot. Considering the impact forces, the system is able to reduce the forces on the robot by 70%. Similarly, Memar and Esfahani [19] used permanent magnets to develop a variable stiffness gripper for handling fragile objects and enhance safety in case of unintentional collisions in industrial applications. Indeed, by controlling the position of magnets, it is possible to regulate the gripper stiffness.

Similarly, the authors have previously presented a design to mitigate the impact of the end-effector when handling objects. A mechanical system composed of a bi-stable mechanism was first designed [20], which guaranteed an instantaneous detection of the impact and delayed the effective force on the robot. Moreover, as the bi-stable mechanism passively reduces the momentum transferred upon collision, the movement range of the impacted objects was limited. This means that the tool could be used to map the environment in the case that a vision system cannot be used or is difficult to implement, as the robot has enough time to elaborate the signals from the sensors without the risk of shooting away the surrounding objects. Alternatively, the authors have recently proposed a hydraulic system [21], with the gripper mounted on the piston of a cylinder, which is connected to a specific hydraulic circuit. Similarly to the bi-stable mechanism, during collisions the gripper moves backward decoupling the dynamics of the robot and of the end-effector. This paper is an extension of the one presented at the IFIT 2022 Conference [21]. The mathematical model of the hydraulic end-effector is improved and integrated with a model that represents the compliance of the robot in the approach direction. The scenarios of possible collisions are widened, considering collisions with fixed obstacles as well. Since the functioning of the hydraulic and bi-stable systems have some similarities, a comparison between the two designs is made in terms of forces on the robot and initial velocity of the impacted object, only one dimension collisions are considered.

The paper is organized as follows: Section 2 presents the mathematical model of the hydraulic end-effector. Section 3 describes the mathematical model of the bi-stable mechanism. Sections 4 and 5 make comparisons between the performances of the two designs in the case of impacts with small objects and fixed obstacles, respectively. Lastly, Section 6 concludes the paper.

2 MATHEMATICAL MODEL OF THE END-EFFECTOR WITH HYDRAULIC SYSTEM

The end-effector equipped with the hydraulic decoupling system is depicted in Figure 1. The gripper is mounted on a piston that slides along the main hydraulic cylinder. The main cylinder is connected to an auxiliary cylinder through an orifice. The auxiliary cylinder is divided into two chambers by a floating piston; the first chamber is filled with oil, whereas the second chamber is filled with pressurized gas.

The compression/expansion of gas in the auxiliary cylinder compensates for the variation in volume caused by the piston motion, hence this layout makes possible the motion of the gripper, since oil is incompressible. The gas inside the auxiliary cylinder not only compensates for the variation in volume, but also makes possible the return of the gripper to the initial position after the collision. The orifice between the two cylinders generates a dissipation of energy that slows

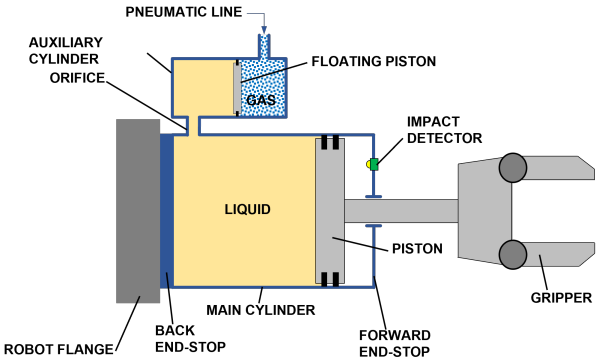

Figure 1 Scheme of the end-effector with the hydraulic compliant system

down both the backwards motion of the gripper after the impact and the rebound toward the initial position.
The hydraulic system is schematized using a non-linear lumped parameter model which is depicted in Figure 2.

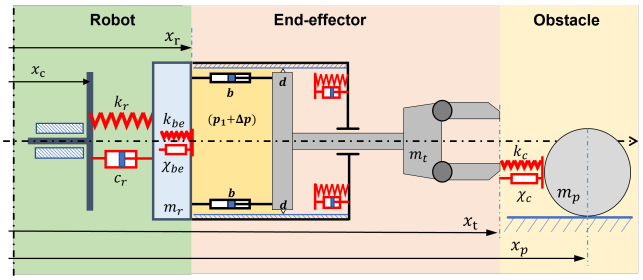

Figure 2 Lumped parameter model of the system.

The variables x_c, x_r, x_t, and x_p are the coordinate of the robot imposed by the control system, the effective coordinate of the robot flange, the gripper coordinate, and the object coordinate, respectively. The mathematical model includes the equation of the adiabatic process of gas, the orifice flow equation, the continuity equation, and the equation of motion of the piston [22]. Pressure p_1 of oil inside the auxiliary cylinder is equal to the pressure of the gas, which undergoes an adiabatic process following the equation:

$$p_1(t) = \frac{p_{10} \cdot V_{g,0}^k}{V_g(t)^k} \tag{1}$$

where p_{10} and $V_{g,0}$ are the initial pressure and volume of the gas; k is the adiabatic constant of the gas ($k = 1.4$); V_g is the effective volume of the gas chamber. It is worth noticing that this equation holds true if the inertia force of the floating piston and the friction forces inside the auxiliary cylinder are negligible, this condition is usually met since the floating piston is small or is replaced by a flexible membrane. The pressure of oil inside the main cylinder is different from p_1 owing to the pressure drop in the orifice, which is given by :

$$\Delta p = CQ^2 sign(Q) \tag{2}$$

where Q is flow rate and C is a global discharge coefficient. Flow rate Q can be calculated by means of the continuity equation:

$$Q = A_p(\dot{x}_r - \dot{x}_t) \tag{3}$$

where A_p is the area of the main cylinder, $\dot{x}_r$ and $\dot{x}_t$ are the velocities of the robot and the gripper respectively. Q is positive if the robot flange velocity is larger than the gripper velocity, i.e. when the volume of oil in the main cylinder is decreasing. The equation of motion of the main piston (connected to the gripper) is:

$$m_t\ddot{x}_t = (p_1 + \Delta p) \cdot A_p - F_c - F_f - F_{f,e} - F_{b,e} \tag{4}$$

in which m_t is the mass of the main piston with gripper. F_f is the friction force between the piston and the cylinder, which includes both a dry friction term (coefficient d) and a viscous term (coefficient b) [22, 23]:

$$F_f = d \cdot \mathrm{sgn}(\dot{x}_t - \dot{x}_r) + b \cdot (\dot{x}_t - \dot{x}_r) \tag{5}$$

F_c is the contact force between the gripper and the object, which is expressed using a non-linear contact model as presented in [20, 24]:

$$F_c = k_c\delta^{3/2} + \chi_c\delta^{3/2}\dot{\delta} \tag{6}$$

where k_c and χ_c are constants and δ is the deformation of the end-effector $\delta = x_t - x_p$ ($x_t - x_p > 0$ guarantees the contact).
$F_{f,e}$ and $F_{b,e}$ are the contact forces due to the impact of the piston with the forward and backward end-stops. These forces are expressed using the same non-linear formulation presented in [25].
The force on the robot due to the collision is calculated as follows:

$$F_r = -(p_1 + \Delta p) \cdot A_p + F_f + F_{f,e} + F_{b,e} \tag{7}$$

The robot joints are not infinitely stiff and force F_r excites the vibrations of the robot, therefore a mathematical model describing the response of the compliant robot to the collision force is needed. To this end, a 1 DOF lumped parameter model of the compliant robot in the approach direction is adopted, see Figure 2. The slider (coordinate x_c) moves along the approach direction according to the law imposed by the control system and is connected to the motors of the robot by an ideal transmission. Since the actual robot is compliant in the approach direction the slider is connected to the end-effector by means of a lumped spring (stiffness k_r) and a lumped damper (damping coefficient c_r). A share

of the mass of the robot (m_r) is added to the end-effector. Actually, the 1 DOF system composed of mass m_r, stiffness k_r and damper c_r represents the vibrations of the robot in the approach direction. The equation of motion of the robot is:

$$m_r\ddot{x}_r = c_r(\dot{x}_c - \dot{x}_r) + k_r(x_c - x_r) + F_r \tag{8}$$

The parameters of the robot model were identified from an actual robot (Omron Adept Viper s650) with the modal analysis approach [20, 26].
If the impacted object has a small mass (m_p) it moves due to the collision and its motion equation is added to the model:

$$m_p\ddot{x}_p = F_c \tag{9}$$

The non-linear analytical model described by equations 4, 8, and 9 was implemented in MATLAB to carry out the simulations presented in the following sections.
When considering the impact with heavy objects (e.g., barriers, tables) which can be considered as fixed obstacles, the model still applies. However, the object is steady, hence x_p is constant.

3 MATHEMATICAL MODEL OF THE END-EFFECTOR WITH BI-STABLE SYSTEM

The mathematical model of the end-effector with the bi-stable mechanism is depicted in Figure 3. This model is similar to the one described in Section 2. The main differences rely on the bi-stable mechanism, which is a chevron-type mechanism [27], equipped with two linear springs of stiffness k_b. The springs are connected to a sliding element, which is constrained to move only in the x direction. Such a sliding element holds the gripper (mass m_t) which interacts with the environment. If no external force is applied to the end-effector, the mass m_t is pushed to the right by the springs.
The forces exerted by the linear springs can be broken up into two components: parallel to the sliding direction and perpendicular to the guide. It is worth noticing that the sum of the latter components is null if the springs are placed in antagonist positions. The force F_b exerted on the robot in the sliding direction is:

$$F_b = -Nk_b(L_0 - L)\frac{x}{L} \tag{10}$$

$$L = \sqrt{H^2 + x^2} \tag{11}$$

where N is the number of springs, L_0 is the initial spring length and L is the actual spring length that is always less than L_0.
Focusing on the detail of the end-effector (Figure 3b) it can be noted that force F_b changes sign along the entire stroke C: if $x > 0$ (i.e., portion C_1) F_b is negative; if $x < 0$ (i.e., portion C_2) F_b is positive. As a result, the end-effector has two stable positions: the first at $x = C_1$, the second

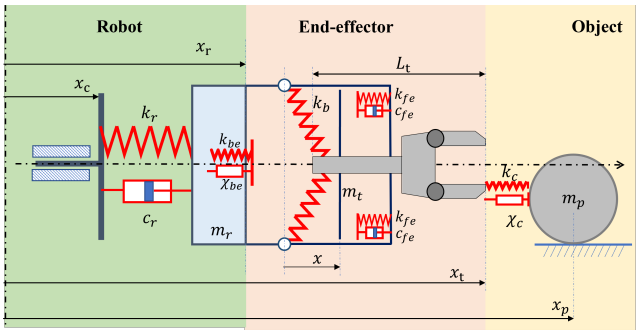

(a)

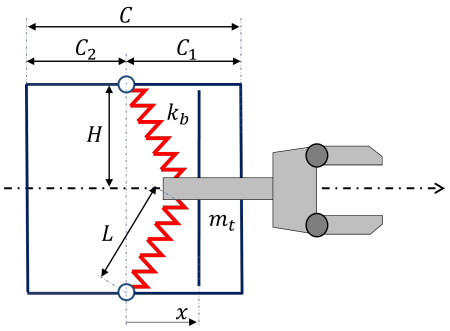

(b)

Figure 3 (a) Lumped mathematical model of the bi-stable mechanism to impact with a small object. The model for the collision with a fixed object is equivalent, but object position x_p is a constant. (b) geometric model of the end-effector.

at $x = -C_2$; in both cases, the springs hold the gripper (mass m_t) pushed against the end stops. The contact forces between gripper, the obstacles, and the end stops are modeled as shown in the previous Section.
Figure 3a shows that the collision between the object and the end effector results in the motion of three elements: the object (x_p) due to the impact; the end effector (x_t) due to the bi-stable mechanism; the robot flange (x_r) due to robot compliance. The equations of motion of these three elements are:

$$m_r\ddot{x}_r = c_r(\dot{x}_c - \dot{x}_r) + k_r(x_c - x_r) + F_b + F_{f,e} + F_{b,e} \tag{12}$$

$$m_t\ddot{x}_t = -F_b - F_c - F_{f,e} - F_{b,e} \tag{13}$$

$$m_p\ddot{x}_p = F_c \tag{14}$$

It is possible to simulate the entire system by imposing an arbitrary input robot trajectory $x_c(t)$.

4 NUMERICAL SIMULATIONS OF IMPACTS AGAINST SMALL OBJECTS

The results of the numerical simulations of the end-effector equipped with the hydraulic system are presented and compared with the ones obtained considering the end-effector with the bi-stable mechanism.

The end-effector approaches the object along a linear trajectory in the horizontal plane driven by the control system. The object is located at distance $x_{p,0}$ from the initial position of the end-effector. A trapezoidal velocity profile is considered and it is characterized by acceleration a_c and deceleration d_c. The collision occurs when the end-effector has reached a constant velocity v_c. It is assumed that the robot stops when the collision is detected, however, the deceleration starts after a time delay DT (dead time), due to the time needed to elaborate the external signal coming from the impact detector (which is installed on the end-effector). The impact detector is represented by an inductive sensor, which switches on when the end-effector detaches of 0.0015 m from the forward end-stop. Table I represents the parameters of the velocity profile and the location of the object. The considered robot is the Omron Adept Viper s650.

Table I - Parameters of the velocity profile and distance of the object from the initial position of the end-effector.

Parameter	Unit	Value
a_c	ms^{-2}	5
d_c	ms^{-2}	9
v_c	ms^{-1}	1
x_{p0}	m	0.2

Table II shows the reduced mass m_r, stiffness k_r and damping c_r of the robot in the approach direction just before the collision (corresponding to configuration $\mathbf{q}$ in the joint space).

Table II - Reduced mass m_r, stiffness k_r and damping c_r just before the collision and the corresponding configuration $\mathbf{q}$ of the robot in the joint space.

Parameter	Unit	Value
m_r	kg	5.2
k_r	Nm^{-1}	$2.19{\cdot}10^5$
c_r	Nms^{-1}	64.7
$\mathbf{q}$	deg	[0 -62 -140 0 -68 0]

In both the considered scenarios (end-effector with hydraulic system and bi-stable mechanism) the parameters of the mathematical model related to the masses m_t, m_p and the contact forces, due to the collisions between the end-effector and the object and the end-stops, are kept constant. These parameters are set as in [21] and are listed in Table III.

Table IV provides the geometrical parameters and mechanical properties of the hydraulic compliant system. L, R_p and R_o represent the stroke of the piston, the radius of the main cylinder and of the orifice, respectively. It is worth noticing that the coefficient d of the dry friction term is set to zero, since it is assumed that the piston moves on a thin film of oil leaked from the oil chamber.

Figure 4 deals with the collision and the reaction of the robot when the dead time is set to $DT = 70$ ms. Figure 4a shows the velocity profiles of the robot control system, robot flange, object and end-effector equipped with the hydraulic compliant system. Figure 4b shows the force on the robot flange. For the sake of simplicity, the force on the robot in Figure 4b and in the following figures is represented as positive when it pushes the robot, although it is negative in the mathematical model.

Table III - Values of the masses of the end-effector and the object and parameters of the contact force models used in the simulations of both scenarios.

Parameter	Unit	Value
m_t	kg	0.048
m_p	kg	0.246
k_c	$Nm^{-1.5}$	$0.6 \cdot 10^6$
χ_c	$Nsm^{0.5}$	$1.35 \cdot 10^6$
k_{be}	$Nm^{-1.5}$	$1 \cdot 10^6$
χ_{be}	$Nsm^{0.5}$	$3.5 \cdot 10^6$
k_{fe}	Nm^{-1}	$1 \cdot 10^6$
c_{fe}	Nms^{-1}	200

Table IV - Geometrical and mechanical parameters of the hydraulic compliant system.

Parameter	Unit	Value
L	m	0.023
R_p	m	0.020
R_o	m	0.008
$V_{g,0}$	m^3	$7.63 \cdot 10^{-5}$
C	kgm^{-7}	16875
p_{10}	Pa	1000
b	kgs^{-1}	0.5
d	N	0

Figure 5 shows the pressure inside the gas chamber during the collision.

The velocity profiles of the robot flange and the end-effector are characterized by vibrations due to robot compliance. These vibrations cause a small perturbation of the velocity profile imposed by the robot control system. The collision drastically reduces the velocity of end-effector and increases the velocity of the object, and they move together after the impact. The oil inside the hydraulic system flows from the main cylinder to the auxiliary cylinder, through the orifice, since the velocity of the robot flange is larger than the one of the gripper. The pressure drop through the orifice leads to a reduction in the relative velocity between the robot flange and the gripper. The robot reacts after a dead time DT, however, the velocity of the end-effector and the object increases above the value of the impact velocity of the end-effector V_c.

Figure 4b shows two main peaks. The first one occurs when the end-effector collides with the object, whereas the

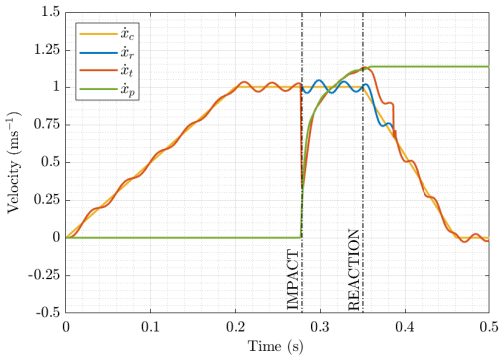

(a)

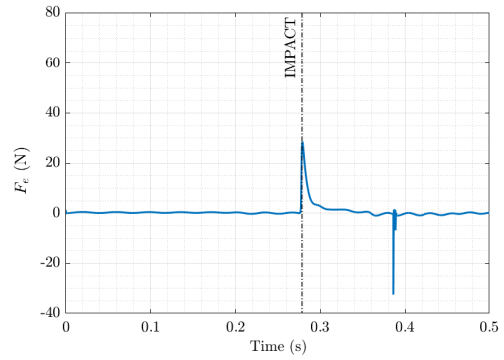

(b)

Figure 4 Numerical results of the collision between the end-effector with the hydraulic system and a small object: (a) velocity profiles of the robot control system, the robot flange, the object and the end-effector equipped with the hydraulic compliant system; (b) force on the robot flange. The dead time is $DT = 70\ ms$.

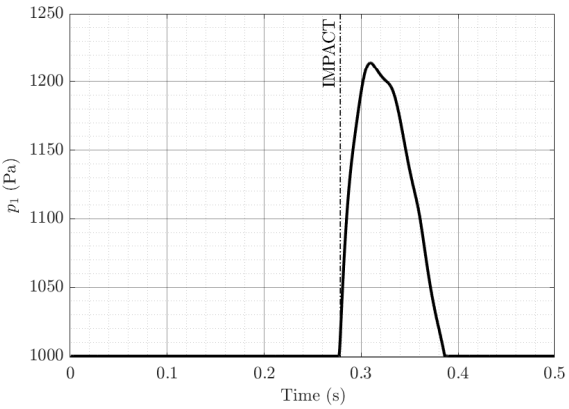

Figure 5 Pressure inside the gas chamber. The dead time is $DT = 70\ ms$.

second one corresponds to the collision between the end-effector and the forward end-stop. Indeed, the end-effector moves towards the forward end-stop after the reaction of the robot, since the velocity of the end-effector is larger that the one of the robot. It is worth noticing that the second peak is negative, since the force acting on the robot during the collision of the end-effector with the forward end-stop pulls the robot.

Figure 5 shows that the pressure in the gas chamber grows quickly after the collision and reaches a peak when the relative velocity between the end-effector and the robot becomes zero. The gas expands when the end-effector moves faster than the robot flange, which means that the oil flow between the chambers reverses.

The simulations carried out considering the end-effector equipped with the bi-stable mechanism are based on the same values reported in Tables I, II, III. The geometrical and mechanical parameters of the bi-stable mechanism are listed in Table V.

Table V - Parameters used to simulate the collision between the end-effector equipped with the bi-stable mechanism and a small object.

Parameter	Unit	Value
L_0	m	0.062
C	m	0.047
$C_1 = C_2$	m	0.0235
N		1
k_b	Nm^{-1}	490
μ		0.12

Figure 6a shows the velocity of the robot control system, the robot flange, the object and the end-effector equipped with the bi-stable mechanism, whereas Figure 6b shows the force on the robot flange during the collision.

Figure 6a shows that the velocity of the end-effector is drastically reduced by the collision, however, in this case, the end-effector and the object move separately. Indeed, the end-effector moves backward toward the back end-stop after the collision, due to the relative velocity between the robot flange and the end-effector and crosses the neutral position of the spring (the crossing corresponds to the local maximum between the two negative peaks of the velocity $\dot{x}_r$). Consequently, the end-effector is pushed backward and collides with the back end-stops. After a first bouncing on the back end-stop, the end-effector reaches a velocity larger than the one of the robot and collides again with the object, which is much slower. This second collision causes several bouncing of the end-effector between the robot flange and the object and leads to a significant increase in the final velocity of the object, which is much larger than V_c.

Figure 6a shows several positive peaks. However, it is important to note that the first collision between the end-effector and the object does not correspond to a peak, since the robot feels only the elastic force of the spring in the bi-stable mechanism. The peaks are related to the collisions

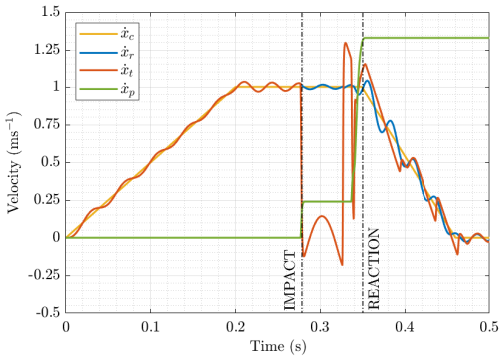

(a)

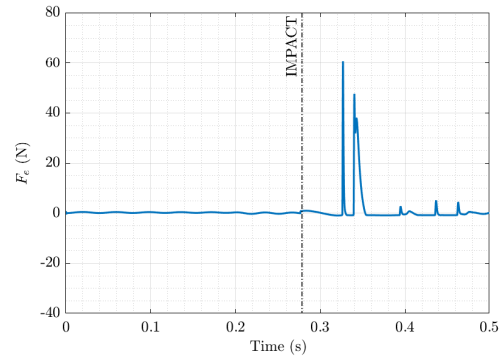

(b)

Figure 6 Numerical results of the collision between the end-effector equipped with the bi-stable mechanism and a small object: (a) velocity profiles of the robot control system, the robot flange, the object and the end-effector; (b) force on the robot flange. The dead time is $DT = 70\ ms$.

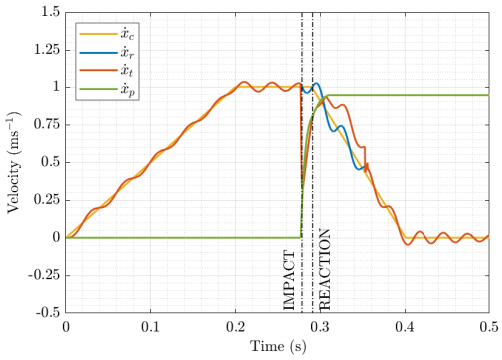

(a)

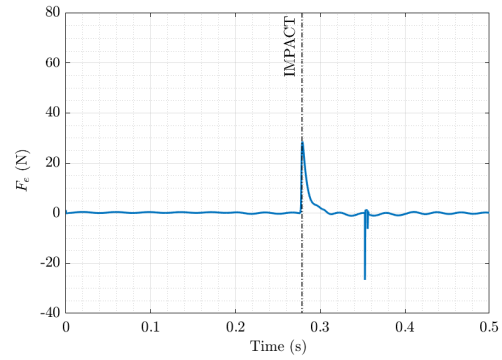

(b)

Figure 7 Numerical results of the collision between the end-effector equipped with the hydraulic compliant system and a small object: (a) velocity profiles of the robot control system, the robot flange, the end-effector and the object; (b) force on the robot flange. The dead time is $DT = 10\ ms$.

between the end-effector and the back end-stop and the object.

This last result highlights the importance of the dead time DT. Hence, further analyses were carried out to analyze the effects of the decrease in the dead-time.

Figures 7 and 8 show the velocity profiles and the force on the robot flange, when the end-effector is equipped with the hydraulic compliant system and the bi-stable mechanism, respectively. In both simulations the dead time is $DT = 10\ ms$.

Figure 7a shows the robot starts decelerating before the relative velocity between the robot and the end-effector becomes zero. Therefore, the final velocity of the object is smaller than the impact velocity V_c. Figure 7b shows that the dead time does not influence the value of the first peak (see Figure 4b), whereas the second one is slightly smaller, since the end-effector has a smaller velocity when the impact with the forward end-stop occurs.

Figure 8a shows that the decrease in DT leads to a significant decrease in the final velocity of the object. Indeed, the faster reaction of the robot avoids the second collision between the end-effector and the object, which reduces the momentum transferred to the object. Moreover, the relative velocity between the robot and the end-effector is smaller when the latter collides against the back end-stop, hence the force applied to the robot flange decreases, as shown in Figure 8b. The comparison of Figures 6b and 8b show that the number of impulses exerted on the robot flange is much smaller when the dead time is shorter.

5 NUMERICAL SIMULATIONS OF IMPACTS AGAINST FIXED OBSTACLES

In this section the dynamics of the end-effector equipped with the hydraulic compliant system and the bi-stable mechanism are compared when the end-effector collides with a fixed obstacle located along the robot trajectory. The robot trajectory is defined as in the previous section, however the impact velocity v_c is reduced to 0.25 ms^{-1} because collisions with fixed obstacles are generally more dangerous than collisions against small objects. Table VI summarizes

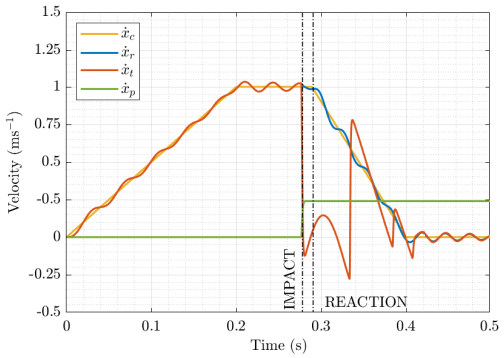

(a)

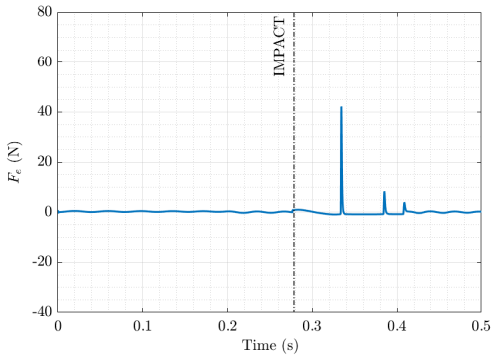

(b)

Figure 8 Numerical results of the collision between the end-effector equipped with bi-stable mechanism and a small object: (a) velocity profiles of the robot control system, the robot flange, the end-effector and the object (b) force on the robot flange. The dead time is $DT = 10\ ms$.

the characteristics of the robot trajectory and the distance of the obstacle from the initial position of the end-effector.

Table VI - Parameters of the velocity profile and distance of the obstacle from the initial position of the end-effector.

Parameter	Unit	Value
a_c	ms^{-2}	1
d_c	ms^{-2}	2
v_c	ms^{-1}	0.25
x_o	m	0.2

The reduced mass m_r, stiffness k_r and damping c_r of the robot just before the collision are summarized in Table II.
Table VII represents the values of the parameters in the contact force model used in the simulations with both end-effectors. These values are obtained from the experimental validation presented in [25]. It is important to note that the collision parameters are different from the previous scenario since the materials of the objects and the velocity are different.

Table VII - Values of the mass of the end-effector and parameters of the contact force models used in the simulations of both scenarios.

Parameter	Unit	Value
m_t	kg	0.048
k_c	$Nm^{-1.5}$	$0.6 \cdot 10^5$
χ_c	$Nsm^{0.5}$	$9 \cdot 10^4$
k_{be}	$Nm^{-1.5}$	$2.25 \cdot 10^6$
χ_{be}	$Nsm^{0.5}$	$3.15 \cdot 10^7$
k_{fe}	Nm^{-1}	$2.25 \cdot 10^6$
c_{fe}	Nms^{-1}	235

The geometrical and mechanical parameters of the hydraulic compliant system are presented in Table IV.
In Figure 9 a rather long dead time is considered ($DT = 70\ ms$). Figure 9a shows the velocity profiles of the robot control system, the robot flange and the end-effector equipped with the hydraulic compliant system. Figure 9b shows the force on the robot flange.
Figure 9a shows that the end-effector stops against the obstacle and remains in contact with it, due to the increase in pressure inside the gas chamber. As shown in Figure 9b, firstly the force on the robot increase, then, it has a slight decrease when the robot brakes. The reduction in the relative velocity between the robot and the end-effector reduces the pressure drop through the orifice, hence the oil pressure on the end-effector. It is interesting to note that the velocity of the end-effector is negative when the robot brakes. Indeed, the contact force pushes backward the end-effector when the force due to the oil pressure decreases, since the end-effector is still in contact with the surface of the obstacle,
The parameters used to simulate the end-effector equipped with the bi-stable mechanism are presented in Table V.
Figure 10a shows the velocity profiles of the robot control system, the robot flange and the end-effector equipped with the bi-stable mechanism, whereas Figure 10b shows the force on the robot flange during the collision. The dead time is $DT = 70\ ms$.
Figure 10a shows that at the beginning of the collision the end-effector decelerates and oscillates, whereas the robot is still moving. The oscillations are related to the robot compliance. The relative velocity between the robot and the end-effector causes the movement of the latter towards the robot flange. When the end-effector crosses the neutral position of the spring, it is pushed against the back end-stop, detaching from the obstacle. Figures 9b shows that at the beginning of the collision the force on the robot is very small. However, the collision between the end-effector and the robot flange applies a very large impulse to the robot. This result highlights that the bi-stable mechanism can reduce the force on the robot only if the crossing of the neutral position is avoided. The reduction of the dead time, which means a

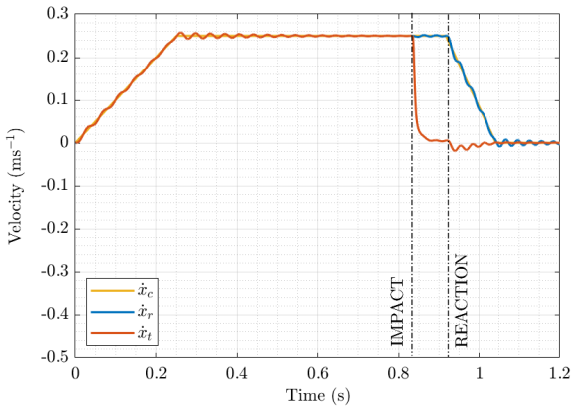

(a)

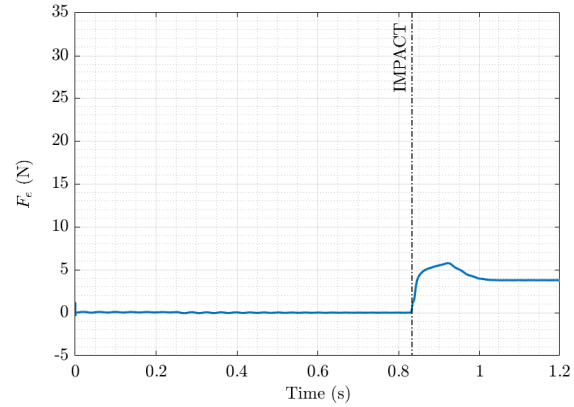

(b)

Figure 9 Numerical results of the collision between the end-effector equipped with the hydraulic compliant system and an obstacle: (a) velocity profiles of the robot control system, the robot flange and the end-effector; (b) force on the robot flange. The dead time is $DT = 70\ ms$.

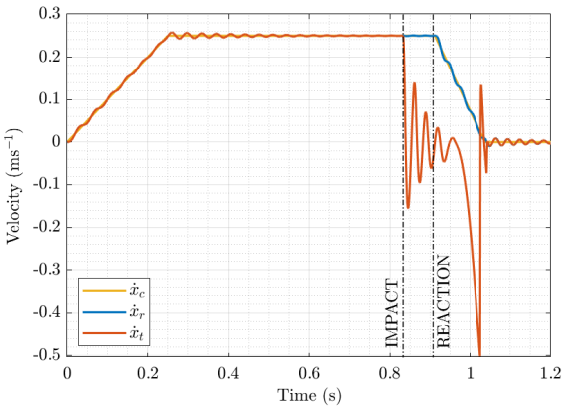

(a)

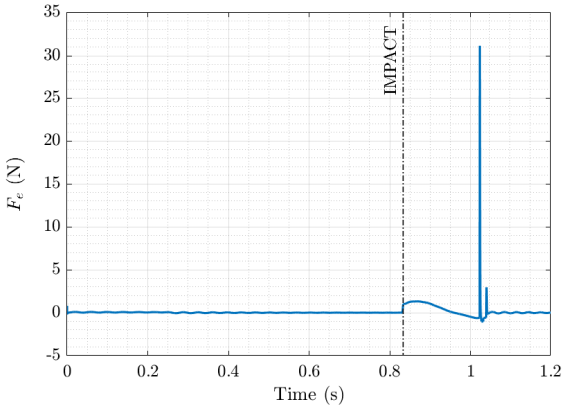

(b)

Figure 10 Numerical results of the collision between the end-effector equipped with the bi-stable mechanism and an obstacle: (a) velocity profiles of the robot control sytem, the robot flange and the end-effector; (b) force on the robot flange. The dead time is $DT = 70\ ms$.

faster reaction of the robot, is an effective solution to this problem, as shown in the following simulations.
Figures 11 and 12 shows the velocity profiles and the force on the robot flange for the end-effector equipped with the hydraulic compliant system and the bi-stable mechanism, respectively, when the dead time is reduced to $DT = 10\ ms$. The velocity profile of the end-effector in Figure 11a is very similar to the one in Figure 9a. Likewise, Figures 9b and 11b show almost the same results. Conversely, the decrease in DT has a significant positive effect on the behaviour of the end-effector with the bi-stable mechanism. Figure 12a shows that the end-effector does not move backwards towards the back end-stop, since the robot stops before the crossing of the neutral position of the spring. Consequently, the impact of the end-effector against the back end-stop is avoided and Figure 12b shows no peaks. It is worth noticing that in this case the force on the robot is slightly smaller that the one obtained when the end-effector is equipped with the hydraulic system.

6 CONCLUSIONS

This paper presented a comparative analysis on two end-effectors designed to mitigate the effects of collisions on the robot with its environments. The analysis was performed using two different mathematical models able to represent the different designs, which are based on a hydraulic system and a mechanical one, respectively. Moreover, the models were used to study two different scenarios, i.e., the impact against small objects and against fixed obstacles.
The analysis of impacts against small objects shows that the end-effector equipped with the hydraulic system presents only an initial peak in the force, which rapidly decreases, and is followed by a second peak due to the impact with the forward end-stop. On the other hand, the bi-stable

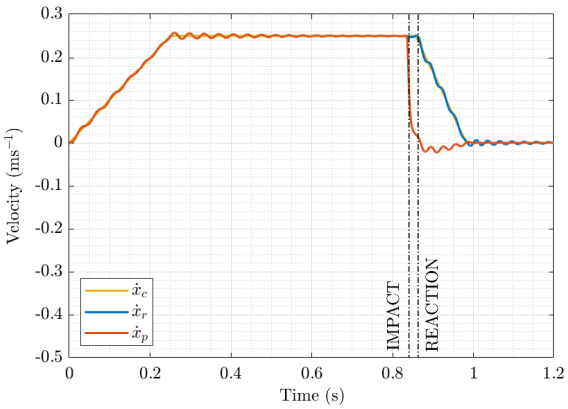

(a)

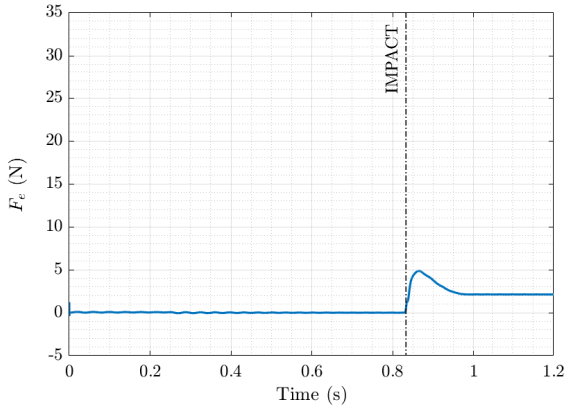

(b)

Figure 11 Numerical results of the collision between the end-effector equipped with the hydraulic compliant system and an obstacle: (a) velocity profiles of the robot control sytem, the robot flange and the end-effector; (b) force on the robot flange. The dead time is $DT = 10\ ms$.

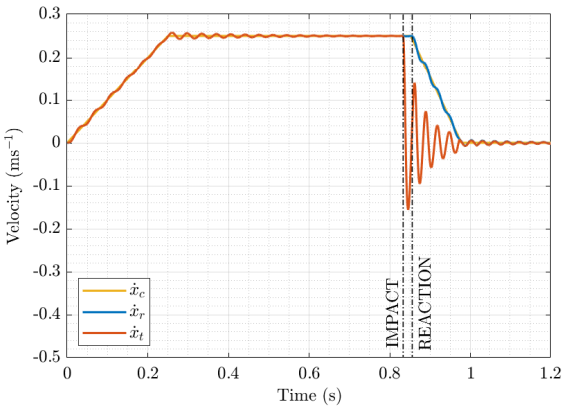

(a)

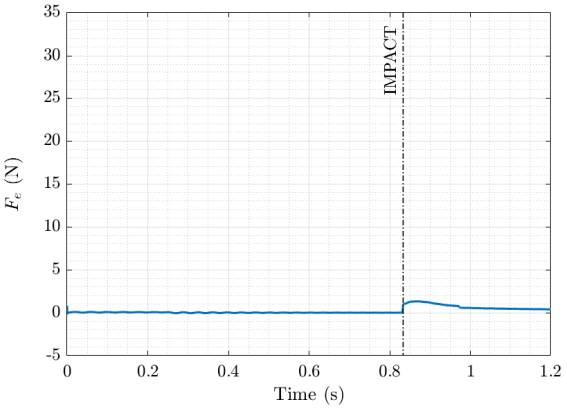

(b)

Figure 12 Numerical results of the collision between the end-effector equipped with the bi-stable mechanism and an obstacle: (a) velocity profiles of the robot control sytem, the robot flange and the end-effector; (b) force on the robot flange. The dead time is $DT = 10\ ms$.

mechanism shows several peaks in the force, due to the end-effector bouncing between the robot flange and the object, leading to higher velocities of the object in comparison to the hydraulic system. Simulations carried out with faster reaction times showed that it is possible to mitigate this last effect.

A similar behaviour is shown when considering the impact against a fixed obstacle. The hydraulic end-effector shows that the force on the robot is only due to the increase in the gas pressure, with the gripper always in contact with the surface. On the other hand, the gripper connected with the bi-stable mechanism is subjected to strong oscillations, leading to higher force transferred to the robot. Again, if the reaction time is reduced, the bi-stable mechanism exerts lower forces on the robot.

The hydraulic system is more complex and requires more precise and costly manufacturing processes than the mechanical system (e.g. the machinery of mechanical seals). Therefore, it is recommended when the reaction time is long and the bi-stable mechanism does not guarantee a relevant reduction in the force transmitted to the robot.

Future developments will include the experimental validation of the hydraulic model and the development of end-effectors based on the same principle, but able to withstand collisions along 2 or 3 directions, e.g., placing two devices in series.

REFERENCES

[1] Y. Cohen, S. Shoval, M. Faccio, and R. Minto. Deploying cobots in collaborative systems: major considerations and productivity analysis. *Int. J. of Production Research*, 0(0):1–17, 2021.

[2] S. Seriani, P. Gallina, L. Scalera, and V. Lughi.

Development of n-DoF Preloaded Structures for Impact Mitigation in Cobots. *J. of Mechanisms and Robotics*, 10(5), 07 2018.

[3] G Cipriani, M Bottin, G Rosati, and M Faccio. A radial basis functions approach to collision avoidance in collaborative tasks. *IFAC-PapersOnLine*, 55(2):307–312, 2022.

[4] Leonardo Sabatino Scimmi, Matteo Melchiorre, Mario Troise, Stefano Mauro, and Stefano Pastorelli. A practical and effective layout for a safe human-robot collaborative assembly task. *Applied Sciences*, 11(4), 2021.

[5] Matteo Bottin, Giulio Rosati, and Giulio Cipriani. Iterative path planning of a serial manipulator in a cluttered known environment. In *The International Conference of IFToMM ITALY*, pages 237–244. Springer, 2020.

[6] Giulio Cipriani, Matteo Bottin, and Giulio Rosati. Applications of learning algorithms to industrial robotics. In *The International Conference of IFToMM ITALY*, pages 260–268. Springer, 2020.

[7] David Baiden and Oleg Ivlev. Separate adjustment of torque and stiffness for pneumatic robot actuators with antagonistic rotary elastic chambers. *International Journal of Mechanics and Control*, 16(1):39 – 48, 2015.

[8] Patrick Dills, Alexander Dawson-Elli, Kreg Gruben, Peter Adamczyk, and Michael Zinn. An investigation of a balanced hybrid active-passive actuator for physical human-robot interaction. *IEEE Robotics and Automation Letters*, 6(3):5849–5856, 2021.

[9] Gill A Pratt and Matthew M Williamson. Series elastic actuators. In *Proceedings 1995 IEEE/RSJ International Conference on Intelligent Robots and Systems. Human Robot Interaction and Cooperative Robots*, volume 1, pages 399–406. IEEE, 1995.

[10] Younsse Ayoubi, Med Amine Laribi, Said Zeghloul, and Marc Arsicault. V2som: A novel safety mechanism dedicated to a cobot's rotary joints. *Robotics*, 8(1):18, 2019.

[11] Antonio Bicchi, Giovanni Tonietti, Michele Bavaro, and Marco Piccigallo. Variable stiffness actuators for fast and safe motion control. In *Robotics research. The eleventh international symposium*, pages 527–536. Springer, 2005.

[12] M. Dežman and A. Gams. Optimization and analysis of the modified plvl-variable stiffness actuator. *International Journal of Mechanics and Control*, 20(1):23 – 33, 2019.

[13] J Sandoval, MA Laribi, and S Zeghloul. Prismatic compliant joint for safe cobots. In *IFToMM World Congress on Mechanism and Machine Science*, pages 1899–1907. Springer, 2019.

[14] S Seriani, P Gallina, L Scalera, and V Lughi. Development of n-dof preloaded structures for impact mitigation in cobots. *Journal of Mechanisms and Robotics*, 10(5):051009, 2018.

[15] Wenzheng Heng, Geng Yang, Gaoyang Pang, Zhiqiu Ye, Honghao Lv, Juan Du, Guodong Zhao, and Zhibo Pang. Fluid-driven soft coboskin for safer human–robot collaboration: Fabrication and adaptation. *Advanced Intelligent Systems*, 3(3):2000038, 2021.

[16] Roman Weitschat, Jörn Vogel, Sophie Lantermann, and Hannes Höppner. End-effector airbags to accelerate human-robot collaboration. In *2017 IEEE international conference on robotics and automation (ICRA)*, pages 2279–2284. IEEE, 2017.

[17] Matteo Pantano, Adrian Blumberg, Daniel Regulin, Tobias Hauser, José Saenz, and Dongheui Lee. Design of a collaborative modular end effector considering human values and safety requirements for industrial use cases. In *Human-Friendly Robotics 2021: HFR: 14th International Workshop on Human-Friendly Robotics*, pages 45–60. Springer, 2022.

[18] Sri Sadhan Jujjavarapu, Hemanth Manjunatha, and Ehsan Tarkesh Esfahani. A variable stiffness end-of-arm tooling mechanism to enhance dynamic task capabilities of robotic manipulators. *Journal of Mechanisms and Robotics*, 15(6):061003, 2023.

[19] Amirhossein H Memar and Ehsan Tarkesh Esfahani. A robot gripper with variable stiffness actuation for enhancing collision safety. *IEEE Transactions on Industrial Electronics*, 67(8):6607–6616, 2019.

[20] Domenico Tommasino and et al. Effect of end-effector compliance on collisions in robotic teleoperation. *Applied Sciences*, 10(24), 2020.

[21] Giulio Cipriani, Domenico Tommasino, Matteo Bottin, Alberto Doria, and Giulio Rosati. Development of a hydraulic system for the mitigation of end-effector collisions. In *Advances in Italian Mechanism Science: Proceedings of the 4th International Conference of IFToMM Italy*, pages 185–192. Springer, 2022.

[22] V. Cossalter and et al. On the non-linear behaviour of motorcycle shock absorbers. *Proc. of the Institution of Mech. Eng., Part D: J. of Automobile Engineering*, 224(1):15 – 27, 2010.

[23] Vittore Cossalter, Alberto Doria, Roberto Pegoraro, and Luca Trombetta. Testing and modelling of an advanced motorcycle shock absorber. *ASME 2010 10th Biennial Conference on Engineering Systems Design and Analysis, ESDA2010*, 3:93 – 102, 2010.

[24] Luka Skrinjar, Janko Slavič, and Miha Boltežar. A review of continuous contact-force models in multibody dynamics. *International Journal of Mechanical Sciences*, 145:171 – 187, 2018.

[25] Domenico Tommasino, Matteo Bottin, Giulio Cipriani, Alberto Doria, and Giulio Rosati. Development and validation of an end-effector for mitigation of collisions. *Journal of Mechanical Design, Transactions*

of the ASME, 144(4), 2022.

[26] Alberto Doria and et al. Analysis of the compliance properties of an industrial robot with the mozzi axis approach. *Robotics*, 8(3), 2019.

[27] Il-Han Hwang, Yu-Seok Shim, and Jong-Hyun Lee. Modeling and experimental characterization of the chevron-type bi-stable microactuator. *Journal of Micromechanics and Microengineering*, 13(6):948, 2003.